International Journal of Climatology
Special Edition: IV ENSO Conference

Submission deadline (extended): June 24th 2019

The role of ENSO flavors and TNA on recent droughts over Amazon forests and the Northeast Brazil region

JC Jimenez[1], JA Marengo[2], LM Alves[3], JC Sulca, K Takahashi[5], S Ferrett[6], M Collins[7]

[1]University of Valencia, Spain
[2]CEMADEN, Brazil
[3]INPE, Brazil
[4]SENHAMI, Peru
[5]IGP, Peru
[6]University of Reading, UK
[7]University of Exeter, UK

Abstract

Amazon tropical forests and the semiarid Northeast Brazil (NEB) region have experienced severe droughts during the last two decades, with a frequency that may have exceeded natural climate variability. Severe droughts impact the physiological response of Amazon forests decreasing the availability to absorb atmospheric CO_2, as well as biodiversity and increasing risk of fires. Impacts of droughts over NEB region are related to water and energy security and subsistence agriculture. Most drought episodes over Amazonia and NEB have been mainly associated to El Niño (EN) events and/or anomalous warming over the Tropical North Atlantic (TNA). However, not all the dry episodes showed a characteristic pattern linked to EN or TNA events. Even in the case of dry episodes linked to EN events, spatial patterns of precipitation anomalies show distinct features depending on EN type (Central-Pacific vs Eastern-Pacific EN). This paper discusses the effects of CP and EP EN events, and the role of warm TNA events on tropical Walker and Hadley circulation leading to drought over Amazonia and NEB regions. [TO BE COMPLETED WITH SOME RESULTS]

1. INTRODUCTION

Together with global and regional warming, the last two decades have experienced three major droughts in the Amazon region (2005, 2010, 2016) and a large-scale drought affecting Northeast Brazil (NEB) since 2012 (Marengo et al 2017, 2018; Aragao et al 2018, Alvala et al 2017 and references quoted in). This raises concerns about the resilience of tropical forests in the Amazon and of semi-arid biome in NEB to extreme droughts. The occurrence of these droughts leads to socio-economical impacts over these regions because drought conditions severely disrupts the livelihood of riverine, urban population and the ecological functioning of the forest in the Amazon and of the semiarid region population.

Earlier studies have shown a pattern of negative rainfall anomalies in Amazonia and NEB during El Niño (EN) (Ropelewski and Halpert 1987). In fact, some extreme droughts over Amazonia were linked to El Niño-Southern Oscillation (ENSO) (e.g. 1912, 1925, 1983, 1987, 1998, 2010, 2016) and over NEB (e.g. 1902, 1951, 1958, 1966, 1983, 1987, 1998, 2010, 2016) conditions in the tropical Pacific. However, drought conditions on those two regions are also related to sea surface temperature (SST) anomalies in the Tropical North Atlantic (TNA), or to a combination of both. Droughts associated to EN events and/or a warmer TNA occur because of a suppression of the convection and thus rainfall in various regions of Amazonia and in the semiarid lands of NEB (Andreoli et al. 2006; Jiménez-Muñoz et al. 2016).

While droughts detected in the NEB occurs over semiarid lands, extreme droughts related to EN over Amazonia occur mainly over tropical forests. Overall, these Amazonian droughts affect north-central Amazonia, but the spatial pattern differs from one EN event to another or from one drought year to another. Moreover, not all El Nino events produce extreme drought in Amazonia and/or NEB, as well as all droughts in Amazonia or NEB are not due to EN (Marengo et al 2008, Alvala et al 2017). The non-EN drought in 2005 affected mostly southwestern Amazonia, while EN 2016 aggravated the dry conditions that started in 2012 (a non-El Niño year) in NEB. Each drought event is different in duration, spatial coverage and intensity, and in the case of 2012, droughts conditions in NEB occurred at the time record floods were detected in Amazonia (Marengo et al 2013, Jiménez-Muñoz et al. 2016).

Different patterns have been observed in the tropical Pacific SST anomalies during El Niño events and in the meridional SST gradient in the tropical Atlantic during drought years in Amazonia and Northeast Brazil. Previous studies have suggested different "types" of El Niño (EN flavours) and different "types" of interactions between El Nino and a warm tropical North Atlantic. Therefore, this study aims to explore the regional distribution of drought in Amazon and NEB linked to the different contribution of Eastern Pacific (EP) and central Pacific (CP) SST anomalies, as well as the Tropical North Atlantic (TNA). For this study we use various case studies of droughts events in both regions (1983, 1998, 2005, 2010, 2012 and 2016) developed during both EN and non EN events.

This paper is organized as follows: Section 2 describes the climatic datasets and calculations, in Section 3 we identify the major EN CP and EP types and TNA events, Section 4 includes the analysis of SST and precipitation anomalies, and Section 5 includes the analysis of atmospheric circulation anomalies observed during each event. Section 6

discuss the results obtained in this study and it includes some concluding remarks.

2. MATERIALS AND METHODS

2.1. Datasets

2.1.1. Precipitation

The Climate Hazards Group InfraRed Precipitation with Stations (CHIRPS) version 2.0 was selected in this study to analyze the precipitation anomalies. CHIRPS dataset was developed by the USGS Earth Resources Observation and Science Center in collaboration with the Santa Barbara Climate Hazards Group (CHG) at the University of California. This dataset includes a quasi-global (50S-50N; 180E-180W) gridded precipitation time series from 1981 to present at 0.05º resolution (Funk et al., 2014). CHIRPS was created from different data sources, including the previous precipitation climatology CHPClim, geostationary thermal infrared satellite observations, the Tropical Rainfall Measuring Mission (TRMM) product, atmospheric model rainfall fields from the NOAA CFSv2, and in situ precipitation observations from national and regional meteorological services. CHIRPS dataset was developed for drought monitoring and trend analysis, and it is available at the CHG web portal *http://chg.geog.ucsb.edu/data/chirps/*.

Selection of CHIRPS dataset among other existing datasets was based on previous studies evaluating the performance of this dataset over the tropics (Burton et al., 2018) and some regions of Brazil, including the NEB region (Paredes-Trejo et al., 2017; Paredes-Trejo et al., 2018; Nogueira et al. 2018).

2.1.2. Sea surface temperature

Sea Surface Temperature (SST) fields were obtained from the European Centre for Medium-Range Weather Forecasts (ECMWF) latest atmospheric reanalysis ERA5. This new reanalysis provides higher spatial and temporal resolutions and more recent model and data assimilation system than the previous ERA-interim reanalysis (Albergel et al., 2018). Monthly SST at 0.25º spatial resolution was used in this study.

SST anomalies over the Tropical Central Pacific (CP) and Eastern Pacific (EP) regions were characterized by the C and E indices (Takahashi et al. 2011). E and C indices were provided by the Instituto Geofísico del Perú (IGP, *www.met.igp.pob.pe/dataos/EC.txt*). The advantage of C and E indices versus other indices such as those based on EN4 and EN3 regions is that C, E are poorly correlated, whereas EN3 and EN4 indices are autocorrelated. The oceanic index for characterization of Tropical North Atlantic (TNA) was extracted from "The state of the ocean climate" initiative (*http://sateteoftheocean.osmc.noaa.gov*).

2.1.2. Atmospheric circulation

Wind and geopotential height anomalies at 850 hPa and 200 hPa were obtained from ERA-interim reanalysis (Dee et al. 2011). Divergence fields for latitudinal (10N-30S) and longitudinal (65W-40W) sections were obtained from NCEP/NCAR reanalysis (Kalnay et al. 1996).

2.2. Methodology

Monthly values of both precipitation (CHIRPS) and SST (ERA5) datasets were used in this study, and they were averaged to produce seasonal values for seasons December-January-February (DJF), March-April-May (MAM), June-July-August (JJA), and September-October-November (SON). Precipitation values were converted to mm/day, even if they are provided for a given season. Anomalies were obtained by removing the average value for the reference period 1981-2010. Standardized anomalies were used in some cases, obtained from the ratio between the anomaly and the standard deviation of the reference mean.

The analysis of precipitation anomalies related to different EN or TNA events was performed from linear regression of seasonal precipitation anomalies onto the concurrent seasonal SST index (CP, EP, and TNA) such that

$$PP' = m \times SST'_{index}$$

where *PP'* is seasonal precipitation anomalies at each gridpoint, and SST'_{index} is the standardized seasonal SST index. Period 1981-2016 was used for this analysis. The coefficient *m* represents the strength of the seasonal climate responses that are associated with ENSO-related and TNA-related anomalous SSTs. The significance of the coefficients is tested using a student's t-test at the 95% confidence level. Maps of residual precipitation anomalies (i.e., anomalies not related to any of the E, C, and TNA SST indices) were obtained by subtraction of regressed anomalies to the observed anomalies.

Trend analysis of precipitation and SST anomalies was performed for each grid point from Mann-Kendall analysis (Kendall, 1975) and Sen's method (Sen, 1968). These methods are nonparametric and make no assumptions on distribution of data.

2.3. Study area

The study area (Figure 1a) includes the Amazon forests and the Northeastern Brazil region. Amazon forests were delimited using a land cover map (MODIS product MCD12C1; Strahler et al. 1999) and the "Evergreen Broadleaf Forest" class. This area was divided into four different geographical regions to account for different seasonality, namely, Northwestern (NW), Northeastern (NE), Southwestern (SW) and Southeastern (SE) regions. NEB region was delimited from a shapefile (Lincoln more details???). NEB region includes a variety of land covers, mainly related to arid or semi-arid landscapes.

Seasonal precipitation patterns are markedly different between Amazonia and NEB, and also between different regions over Amazonia (Figure 1b). Roughly, the rainy season over Northern Amazonia occurs during the boreal spring/summer, whereas the dry season occurs during the boreal autumn/winter, and the pattern is approximately reversed over Southern Amazonia. NEB region shows regional variations, with a rainy season over Northern NEB during austral fall and over the coastal region of Eastern NEB during austral winter, and a widespread dry season over the semiarid region austral spring. The amount of maximum precipitation over Amazonia is approximately four times greater than over NEB.

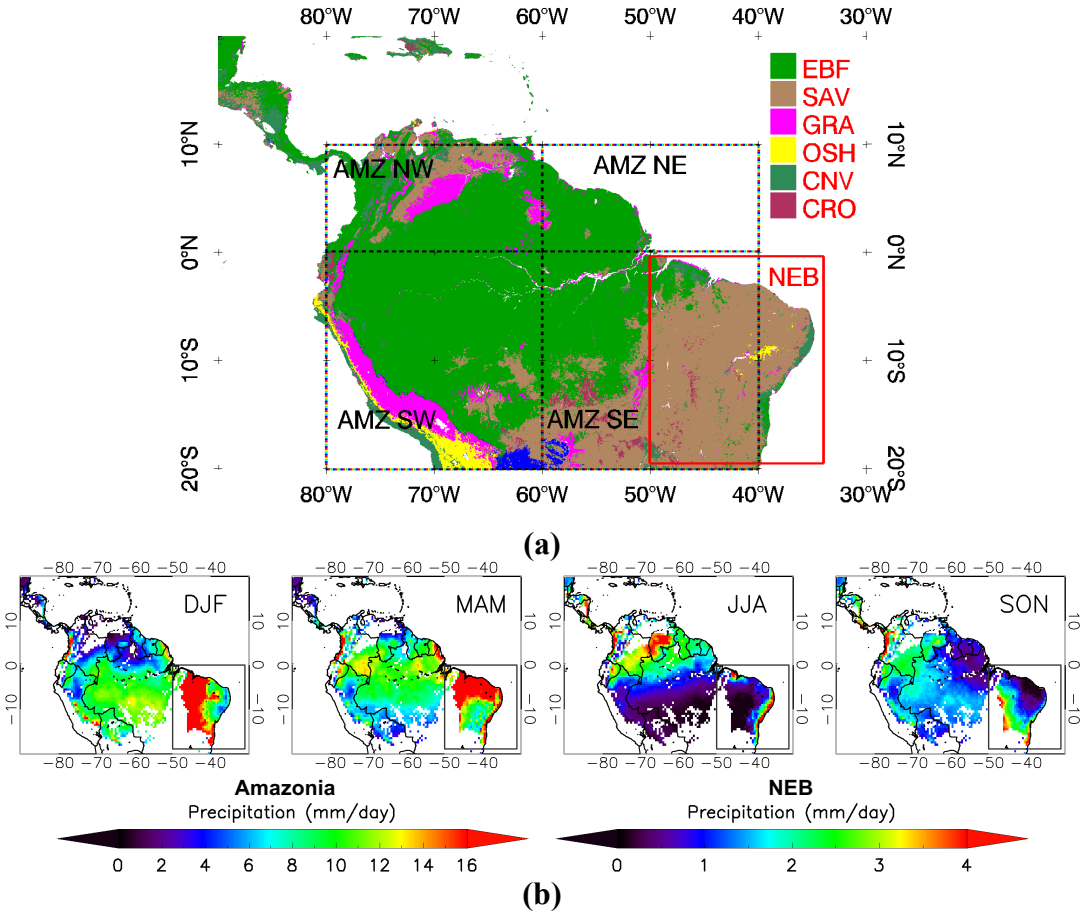

Figure 1. (a) Land cover maps of the study area (EBF: Evergreen Broadleaf Forest; SAV: savanna; GRA: grassland; OSH: Open Shrubland; CNV: Crop and Natural Vegetation; CRO: Cropland). Dashed boxes (in black) indicate the four Amazonian (AMZ) subregions (NW: Northwest, NE: Northeast, SW: Southwest, SE: Southeast). The red box indicates the Northeastern Brazil (NEB) region. **(b)** Climatological mean values (1981-2010) of seasonal (DJF, MAM, JJA, SON) precipitation over the study area. Values are provided in mm/day. Precipitation over NEB was rescaled for visualization purposes.

3. IDENTIFICATION OF INTENSE WARM EP, CP AND TNA EVENTS

We identified different intensities of warm EP, CP and TNA events based on thresholds applied to SST anomalies for E and C indices, and SST anomalies over the TNA region (Table 1). In the case of E and C indices, thresholds were applied to seasonal values for the period DJF. Intensities were categorized into 'weak', 'moderate', 'strong' and 'very strong' using threshold values of 0.5, 1.0, 1.5 and 2.0 ºC, respectively. In the case of TNA SST anomalies, thresholds were applied to seasonal values for the period MAM. Because the magnitude of the anomaly over the TNA is lower than the magnitude of the anomaly over the tropical Pacific, threshold values were reduced to 0.25, 0.5, 0.75 and 1.0 for 'weak', 'moderate', 'strong', and 'very strong' categories, respectively.

Table 1. Thresholds values selected for the categorization of different intensities for warm EP, CP and TNA events. Values refer to sea surface temperature anomalies (SST') in K.

Category	E or C	TNA
Weak	0.5 ≤SST'<1.0	0.25 ≤SST'<0.5
Moderate	1.0≤SST'<1.5	0.5≤SST'<0.75
Strong	1.5≤SST'<2	0.75≤SST'<1.0
Very Strong	SST'≥2.0	SST'≥1.0

Figure 1 shows the temporal evolution of E, C and TNA SST indices, where the different intensity categories are marked. In terms of EP events, 1983 and 1998 were categorized as 'very strong', and 2016 as 'strong'. The most intense CP event in the last seven decades was identified in 2010 (the only 'very strong' event), closely followed by the recent 'strong' event in 2016. Other past 'strong' events were also identified in 1992, 1969 and 1958. The only 'very strong' TNA event was identified in 2010, with a 'strong' event in 2005, and other past 'strong' events in 1969 and 1958. It is remarkable that the number of warm CP events is higher than the number of warm EP events, although most of the CP events were categorized as 'weak' or 'moderate'. The number of warm TNA events was also higher than the number of warm EP events, with sustained warm anomalies almost from 1995 to present.

Spatial patterns of SST anomalies for the strongest warm events are illustrated in Figure 2. The three strongest EN events (1983, 1998, 2016) show high warm SST anomalies peaking in DJF and transition to cold SST anomalies (La Niña conditions) during the JJA season. Some differences are also observed between the three different ENs: 1983 showed a strong warm anomaly near the coast of Peru (EN1+2 region), 1998 provided the coldest SST anomalies over EN region, and 2016 evidenced a widespread warming over adjacent sea regions. SST anomalies over TNA region were neutral to cold in 1983, but neutral to warm in 1998 and 2016. EN conditions were also observed in 1992, where warm SST anomalies were more intense in the CP (EN4 region), similarly to the case of 2016. Events in 2005 and 2010 were characterized by weak EN conditions, with warm SST anomalies focused over the CP (EN4) in DJF, but intense warm SST anomalies over the TNA during MAM and, to lesser extent, in JJA.

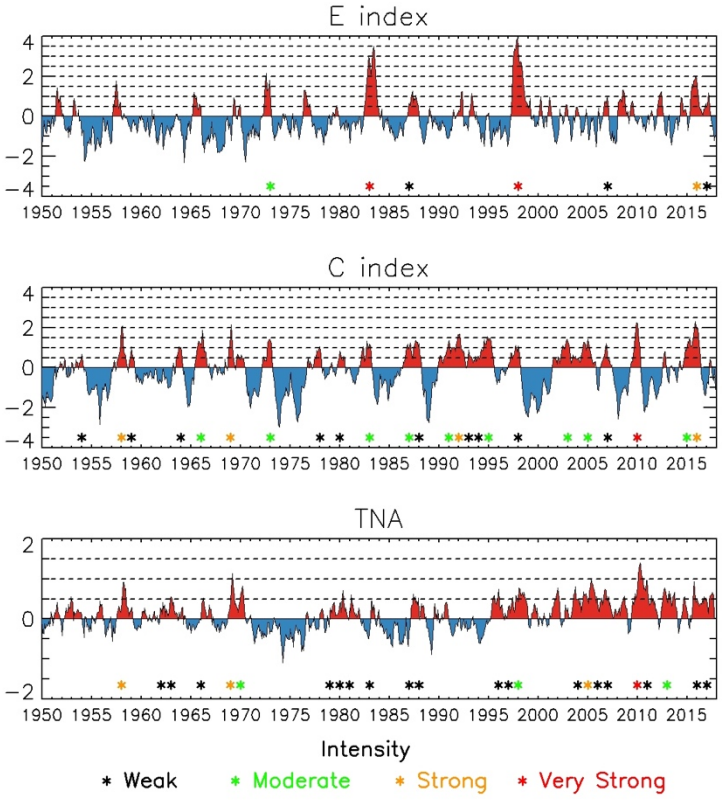

Figure 1. Temporal series of monthly values for E, C and TNA SST indices. The different intensities of particular events were categorized into 'weak', 'moderate', 'strong', and 'very strong' depending on the seasonal value of positive SST anomalies.. The asterisks indicate the year of each event.

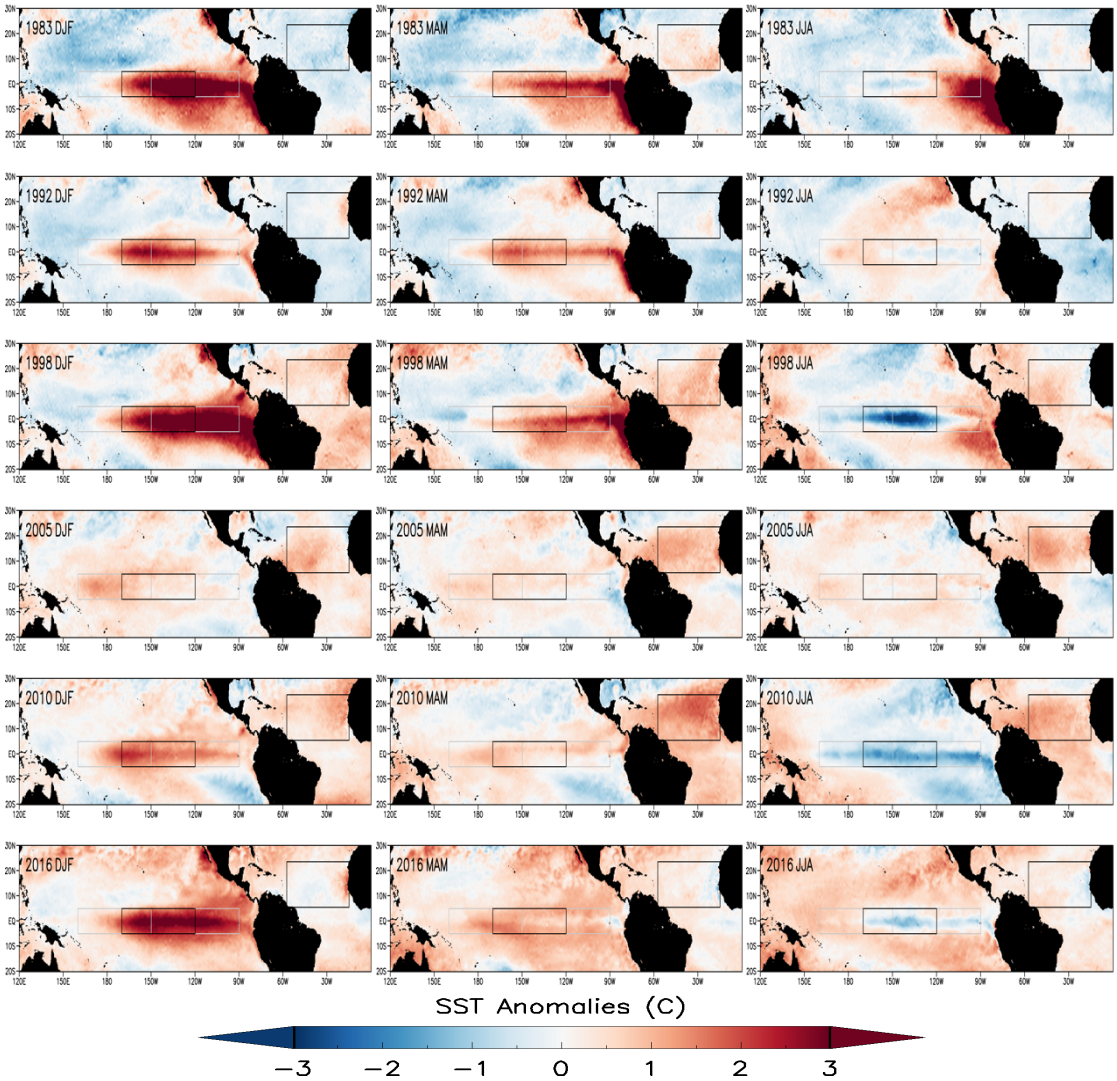

Figure 2. Spatial patterns of seasonal (DJF, MAM and JJA) Sea Surface Temperature (SST) anomalies for different warm EP, CP and TNA events (see Figure 1). The two grey boxes mark EN3 and EN4 region, and black boxes mark EN3.4 and TNA regions.

4. INFLUENCE OF SST ANOMALIES ON PRECIPITATION ANOMALIES OVER AMAZONIA AND NEB REGION

In this section we analyze the precipitation anomalies over Amazonia and NEB regions for the major EN and TNA events shown in the previous section. We focus on the identification of characteristic features linked to EN CP or EP and TNA events, but also on the identification of features or drought episodes that are not linked to EN or TNA events.

4.1. Spatial patterns of precipitation anomalies during EN and TNA events

Figure 3 shows the spatial patterns of precipitation anomalies over Amazon forests and NEB region for the warm EP, CP and TNA events presented in Figure 2.

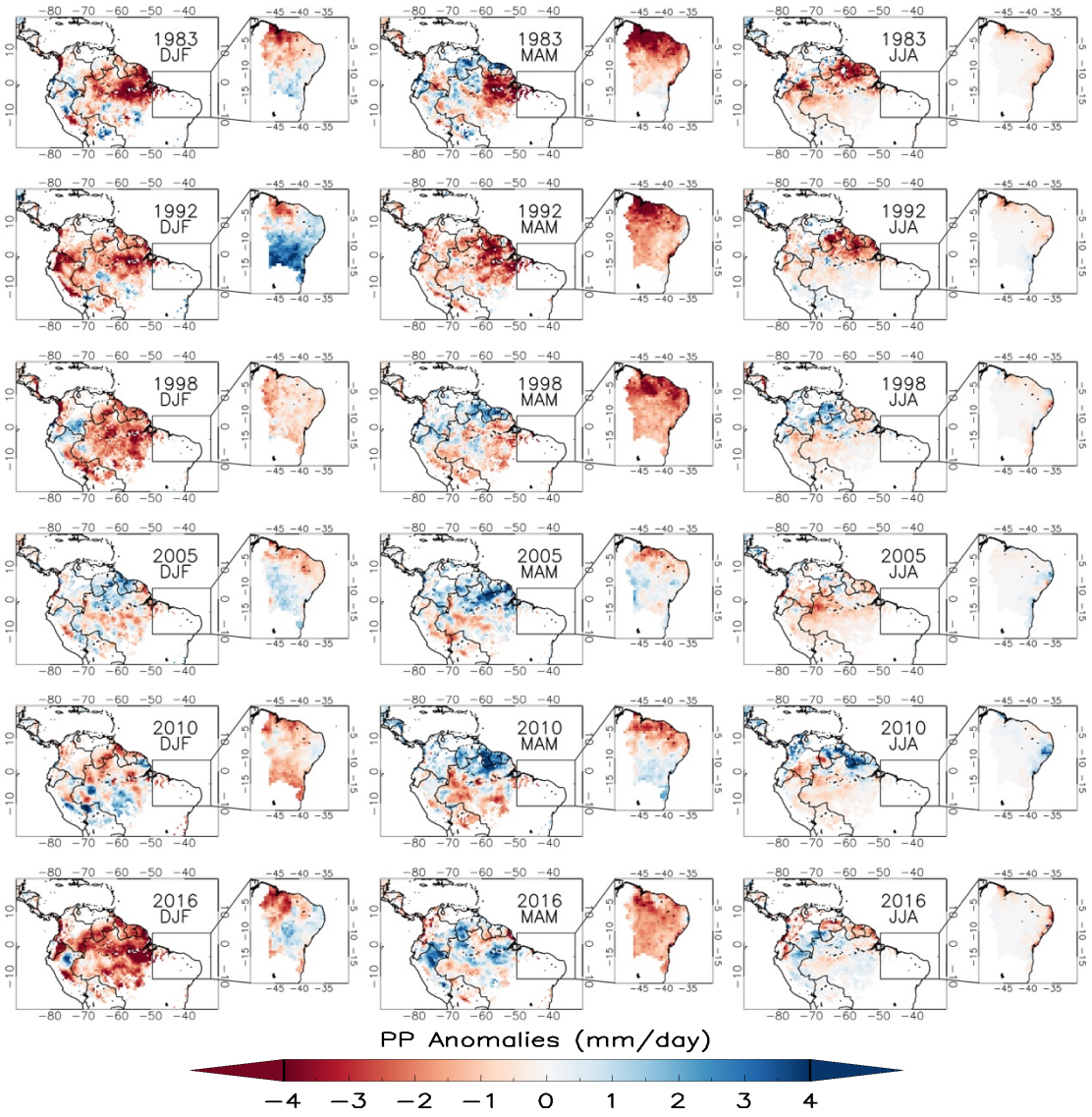

Figure 3. Spatial patterns of precipitation anomalies during seasons DJF, MAM and JJA for different strong EN and TNA events. Values are only displayed over Amazon tropical forests and NEB region. The zoom over the NEB region is marked by a black box for a better visualization.

4.2. Precipitation deficits linked to non-ENSO/non-TNA events

Precipitation deficits presented in the previous section occurred under warm SST anomalies over the tropical Pacific and/or North Atlantic. However, precipitation deficits were also observed under conditions not necessarily linked EN or TNA events, and in some cases these precipitation deficits occurred under cold SST anomalies. Figure 4 shows scatter plots of precipitation (MAM season) and SST (DJF season) standardized anomalies (E, C and TNA indices) over different Amazonian geographical sectors, and Figure 5 includes the scatter plots over the NEB region. Precipitation deficits under cold SST anomalies are represented by yellow circles, with significant dryness (standardized anomalies < -1) represented by filled circles. In the case of Amazonia (Fig. 4), years 1985 and 1988 showed precipitation deficits under cold SST anomalies over some sea regions. Same occurred for NE region in 1986, 1992 and 2009, and SW region in 1983 and 1992.

The SW region did not experience any dry/cold event. NEB region (Fig. 5) experienced dry/cold events in 1990, 1992, 1993 and 2012, with this last year providing the lowest precipitation anomaly in our study period. Figure 6 shows the spatial patterns of SST and PP anomalies for 1990, 1993, 2012.

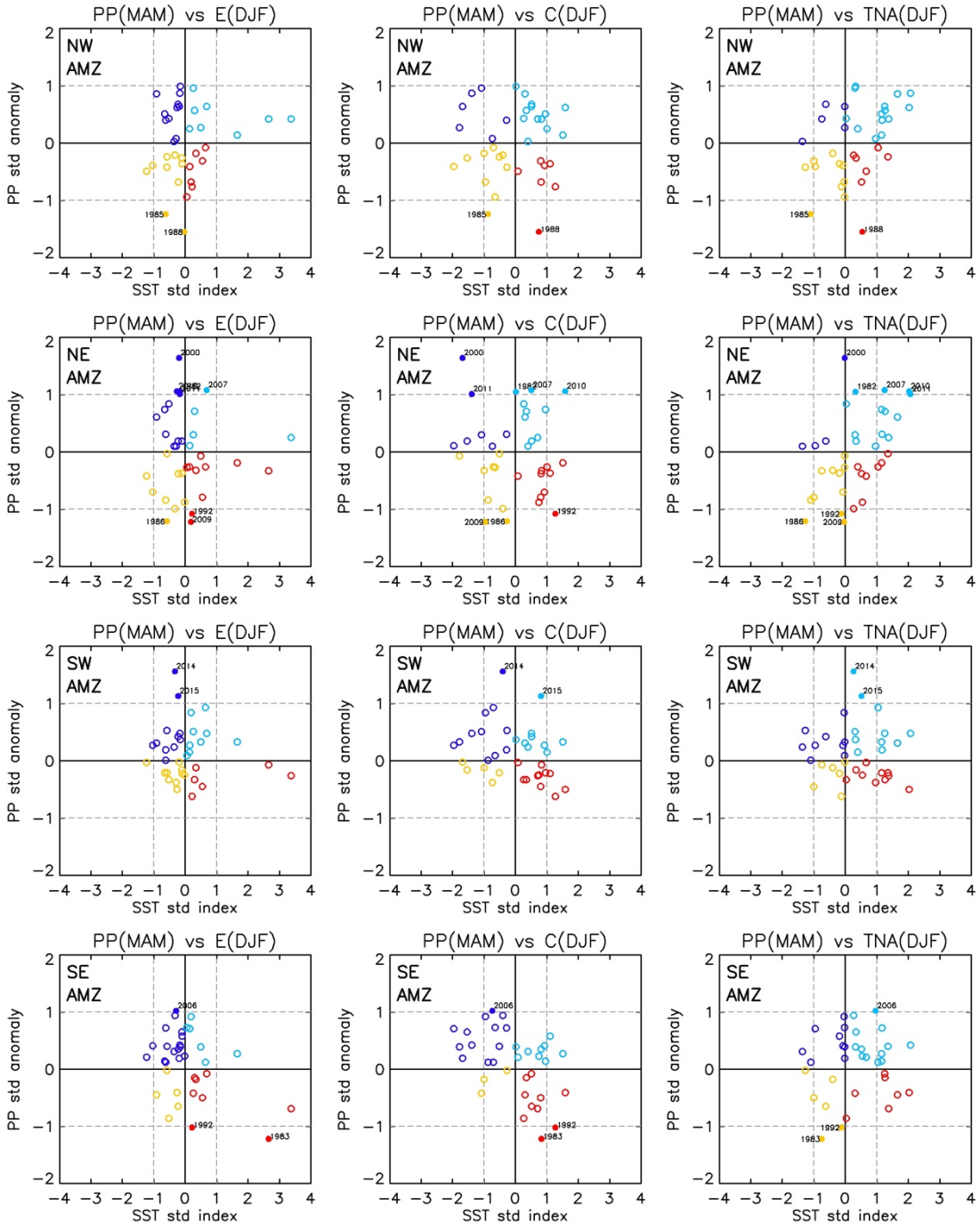

Figure 4. Scatter plots of standardized precipitation (PP) anomalies during the MAM season versus standardized Sea Surface Temperature (SST) anomalies during the DJF season using three SST indices (E, C, TNA) and four regions over Amazonia (NW: Northwest, NE: Northeast, SW: Southwest, SE: Southeast). Dark blue circles indicate wet episodes under cold SST conditions, light blue circles indicate wet episodes under warm SST conditions, yellow circles indicate dry episodes under cold SST conditions, and red circles indicate dry episodes under warm SST condition. Filled circles were used for those cases where PP standardized anomalies exceeded one standard deviation.

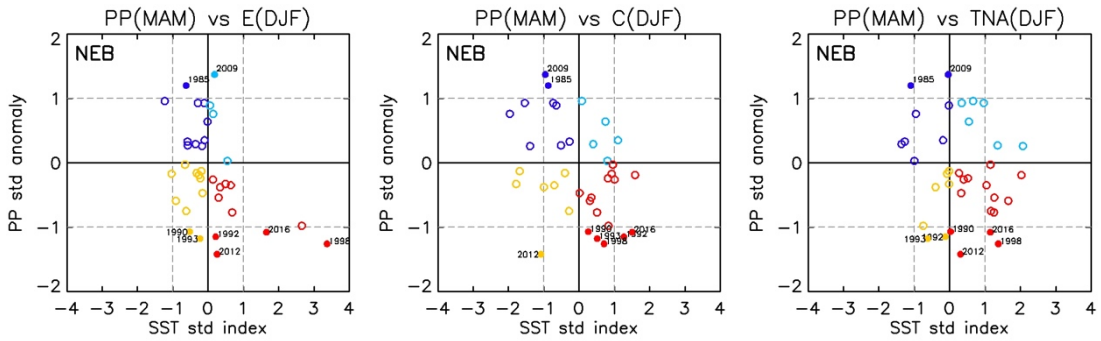

Figure 5. Same as Figure 4, for the Northeastern Brazil (NEB) region.

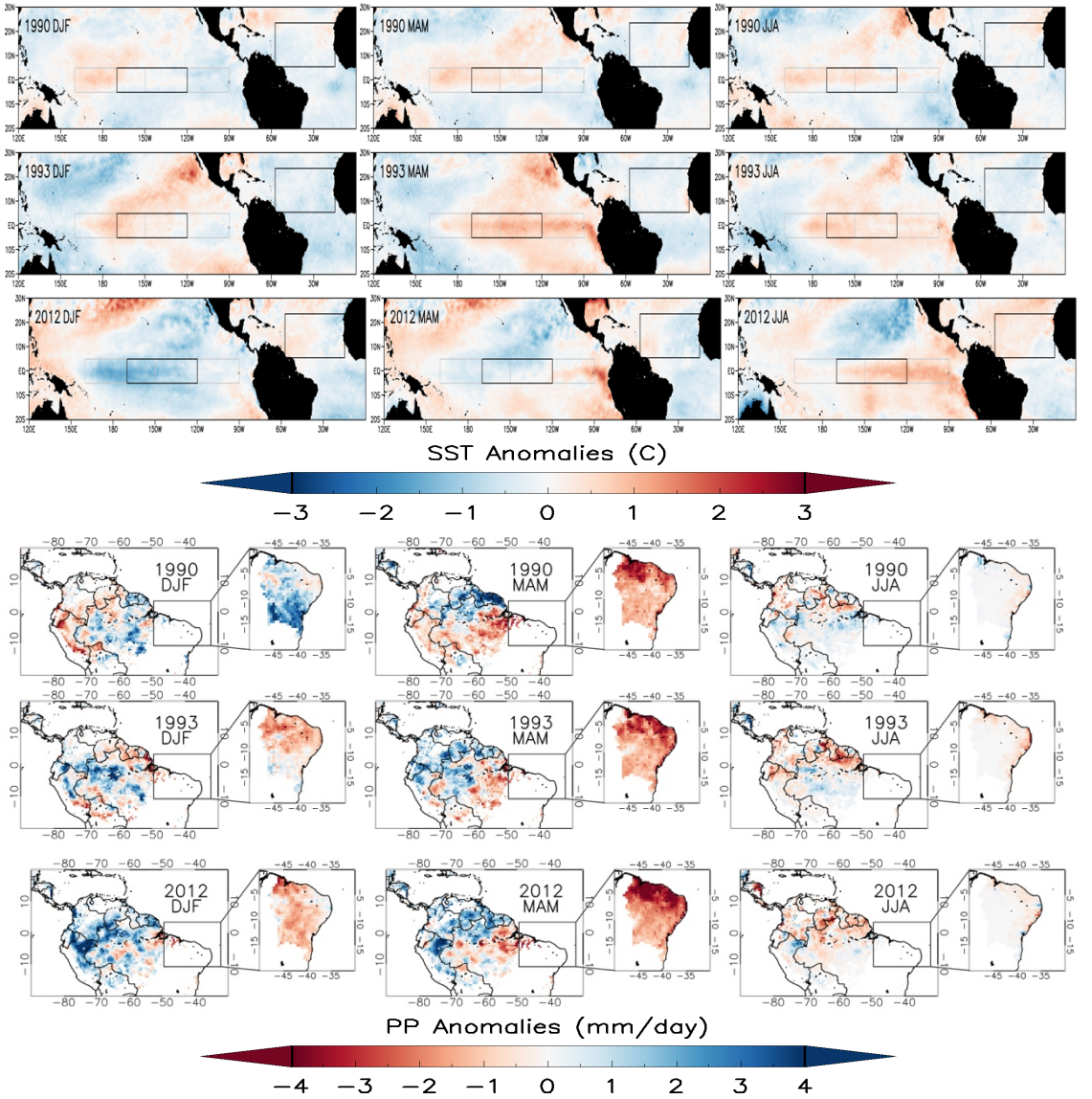

Figure 6. Spatial patterns of Sea Surface Temperature (SST) and precipitation (PP) anomalies during DJF, MAM and JJA seasons for years 1990, 1993, and 2012. These years were not linked to EN neither TNA events, but they are linked to strong precipitation deficits over NEB region.

4.3. Contribution of E, C, and TNA to observed precipitation anomalies

Linear regression analysis was performed over precipitation and SST anomalies in order to better understand the role of the different ENSO flavors (E vs C) and TNA over the observed spatial patterns in Amazonia and NEB. The slope of the regression is presented in Figure 7 for the three SST indices (E, C, TNA) and seasons DJF, MAM and JJA.

During the austral summer El Niño events inhibits precipitation over wide areas of Northeastern Amazonia, with a similar pattern for E and C indices. However, the signal of the C index is stronger than the signal of the E index. In the case of the NEB region the contribution of E and C is only significant over some regions of northern NEB, and again the signal for the C index is stronger than the E index. During the austral winter the role of TNA is not significant.

During the austral spring, the signal of E and C indices are weak over Amazonia, but they become strong over northern NEB, with E index providing a slightly higher signal than the C index. During this period, the signal of TNA over northern NEB is also significant and strong, whereas Amazonia shows a characteristic north-south dipole (wetness over northern Amazonia and dryness over southern Amazonia). The austral winter shows only a weak signal of E, C and TNA indices, whereas the signal almost vanishes over NEB region.

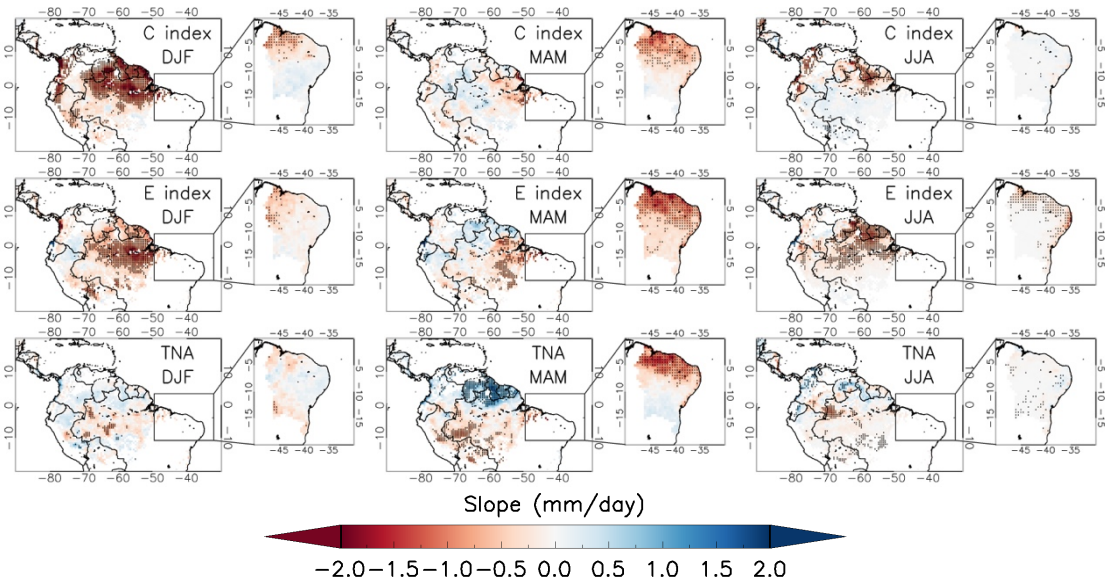

Figure 7. Linear regression coefficient between standardized SST indices (E, C, TNA) and precipitation anomalies for DJF, MAM and JJA seasons. Values are in mm/day per standard deviation. Pixels at the 95% confidence level are marked.

The contribution of the different sea regions can be also analysed through the residuals, once the contribution from E, C and TNA indices are removed from the precipitation anomalies. Results are presented in Figure 8. Overall, a wet pattern arises when E, C and TNA contributions are removed, especially over Amazonia. However, in the case of 2012 over NEB, the dry pattern is similar to the actual precipitation anomalies (Figure 6), confirming a drought event not related to EN or TNA, but with weak La Niña conditions during DJF-2012.

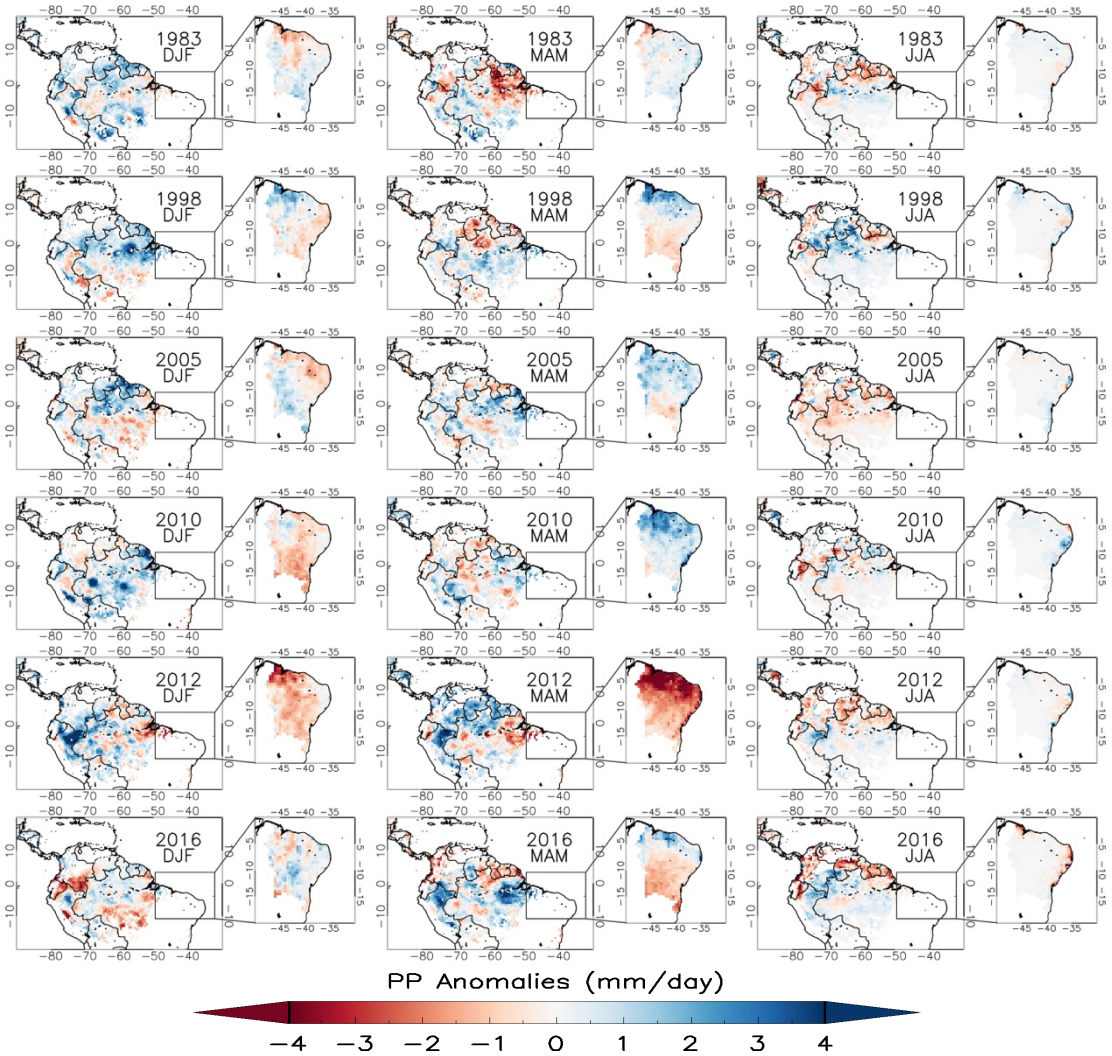

Figure 8. Residuals of precipitation anomalies after removal of contributions from E, C and TNA indices.

4.4. Temporal trends

Time series of monthly precipitation are shown in Figure 9 over Amazonia and NEB regions. Rainfall deficits are observed over particular EN and TNA events, as presented in the previous sections, and it also shows a strong interannual variability of precipitation over these regions. Long-term trends are presented in Figure 10, suggesting a significant wetting trend over northern Amazonia and a significant drying trend over NEB during the boreal spring. For the rest of seasons results are not conclusive.

In terms of SST (Figure 11), EN regions show a slight warming trend but it is not significant. The TNA region shows a significant warming trend for austral spring and summer. A warming trend over TNA is also observed during austral spring and summer.

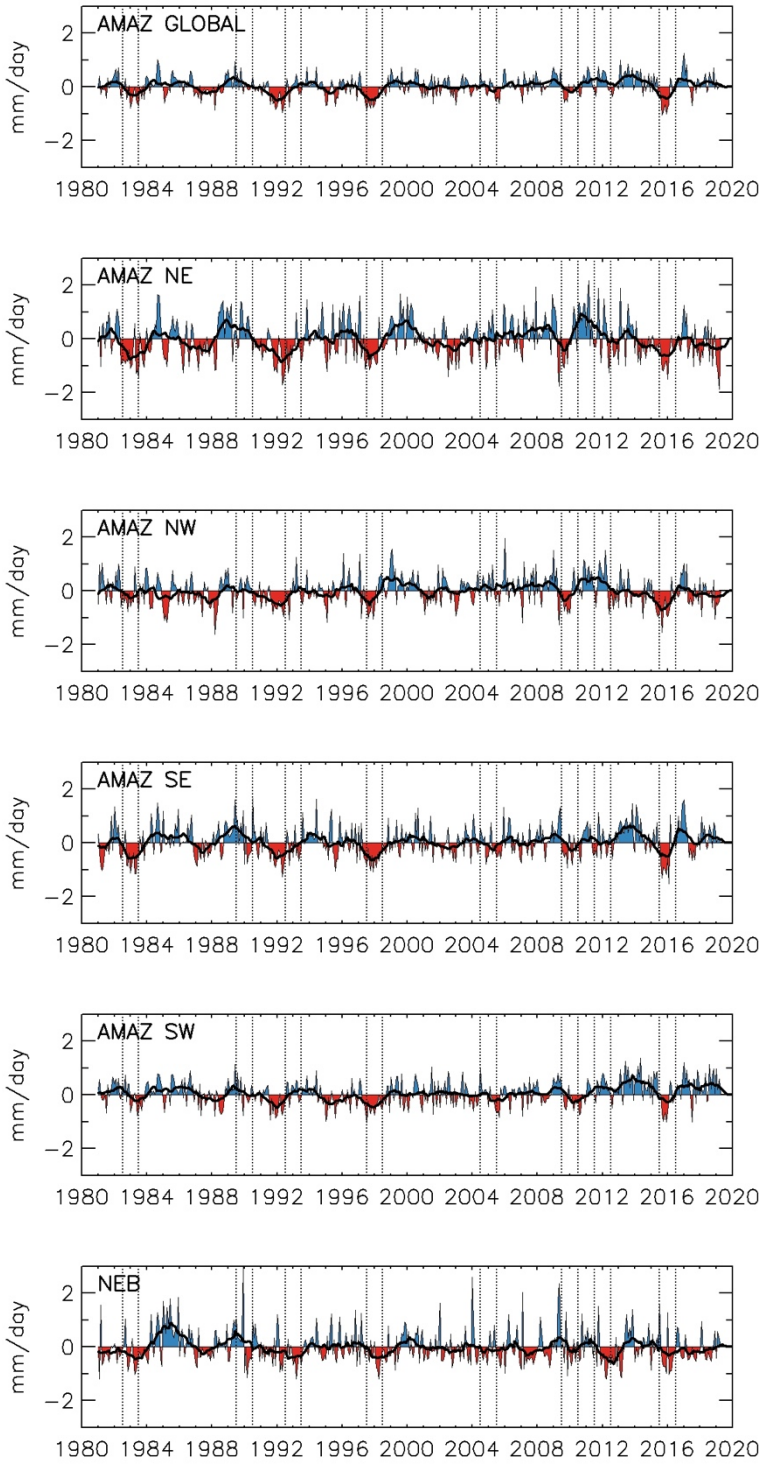

Figure 9. Temporal series of monthly precipitation anomalies (in mm/day) over different Amazonian subregions and the NEB region. 12-month running mean is overplotted.

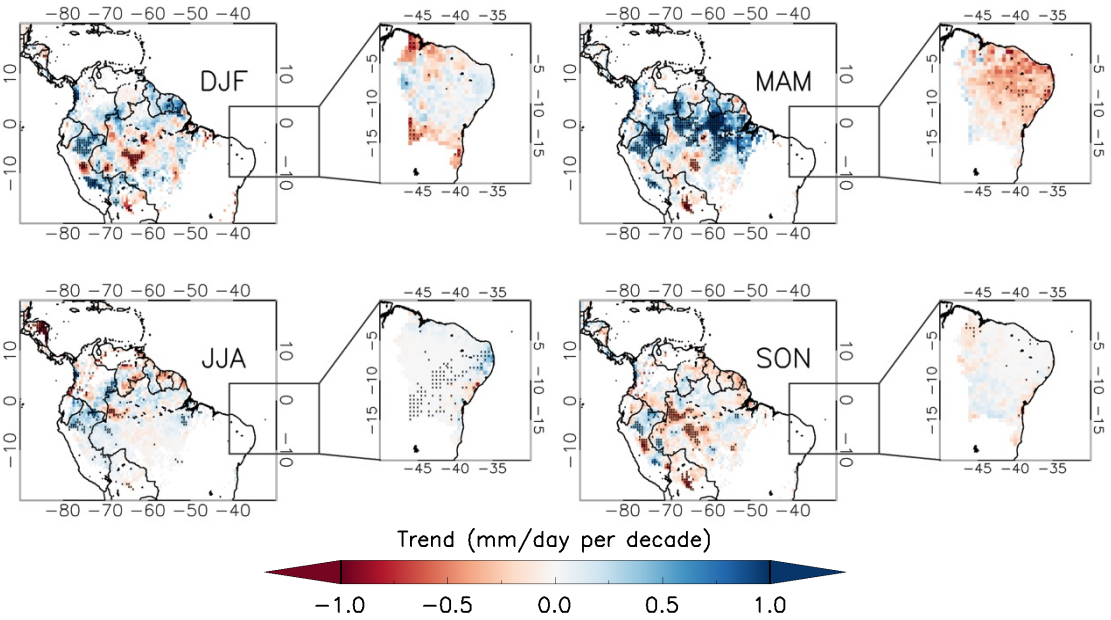

Figure 10. Trends in seasonal (DJF, MAM, JJA, SON) precipitation anomalies for the period 1981-2016. Pixels with values at the 95% confidence level are marked.

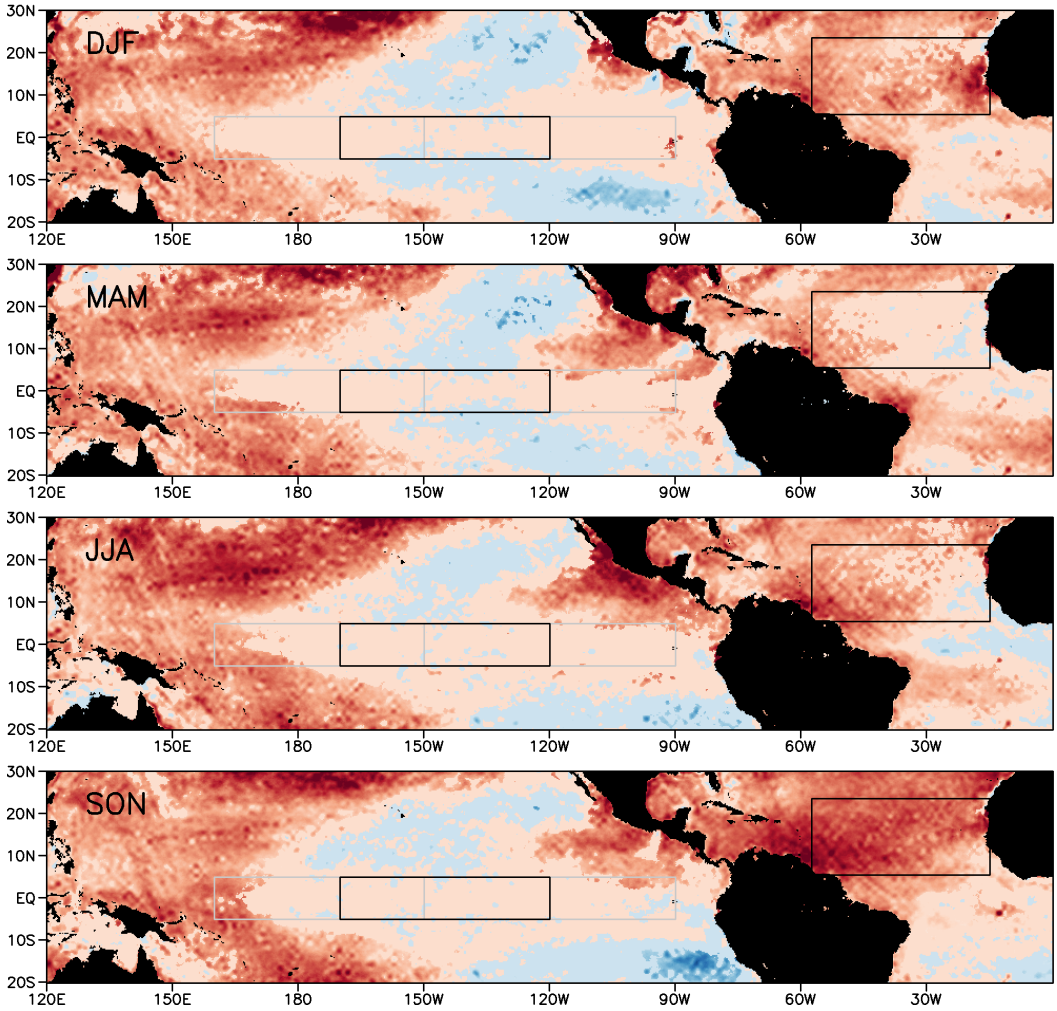

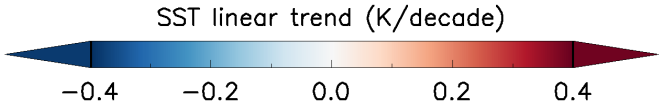

Figure 11. Trends in seasonal (DJF, MAM, JJA, SON) precipitation anomalies for the period 1981-2016. Pixels with values at the 95% confidence level are marked..

5. IMPACTS ON ATMOSPHERIC CIRCULATION

We discuss in here the low level circulation during austral summer DJF and fall MAM in Amazonia and Northeast Brazil for the case studies 1983, 1995, 2005, 2012, 2012 and 2016. MAM is the peak of the rainy season in Northeast Brazil and central-eastern Amazonia. These analyses should be considered in context of the SST and rainfall anomalies from Figures 2 and 3, and the equatorial cross sections of vertical velocity over the Pacific, equatorial South America and the Atlantic sectors from Figure TTT.

Summertime circulation

Changes in large-scale circulation associated with SST patterns are responsible for rainfall anomalies, particularly during austral summer MAM and autumn MAM. In 1983, 1998 and 2016, all during strong El Nino events, changes in atmospheric circulation and rainfall were consistent with the notion of an active role of warmer-than-normal surface waters in the equatorial Pacific during DFJ and in the tropical North Atlantic in MAM 1983 and in both DJF and MAM in 1998 and 2016 (Figure …). Low-level atmospheric circulation anomalies in the Amazon and Northeast Brazil regions show weakened northeast trades into tropical South America, determining less rainfall and drought conditions in both regions.

In 2005, the causes of the drought were not related to El Niño but to an anomalously warm tropical North Atlantic, and near-surface circulation and moisture transport from the tropical Atlantic into southwestern Amazonia was reduced during the onset and peak of the summertime rainy season in 2005 in DJF and MAM, respectively.

The trade winds over the tropical Pacific were weakened in 2010 consistent with El Nino. Anomalously warm tropical North Atlantic mainly in MAM determined weakened Northeast trades over the tropical North Atlantic a d . The ITCZ was located anomalously northward displaced of its climatic position, by about 5° over equatorial Amazonia. At 10 °S there is a strong flow from the Northeast coming from an intensified and northward displaced subtropical Atlantic high.

In 2012, there was a unique situation since both the Amazon and Northeast Brazil showed contrasting rainfall patters. The Atlantic moisture enters into the western part of Amazonia then turning southward to the southern Amazonia region, where the Chaco low was intensified. This was favored by the intensification of subtropical high pressure over the region, associated with an anomalously intense and northward-displaced Atlantic high over a relatively colder subtropical South Atlantic Ocean (Marengo et al 2013). This pattern observed in 2012 was not found during other wet years in Amazonia such as 1989, 1999, and 2009. This suggests La Nina as the main cause of the abundant rainfall in western Amazonia from October to December, with wet conditions starting earlier and

remaining until March 2012, mostly in northwestern Amazonia. In Northeast Brazil, the dry conditions started to appear in December 2011 in the northern sector and then extended to the entire region by the peak of the rainy season of February–May 2012, with the Northeast trades weakened during austral summer and suggesting an anomalously northward displaced ITCZ.

The zonal and meridional vertical circulation cross-sections in Figures x and 2x are consistent with surface wind anomalies and with SST anomalies. Subsidence anomalies appear over areas with negative rainfall anomalies over Amazonia and Northeast Brazil during drought and EN years, with convection and intense rainfall over warm SST in the eastern Pacific region. Upper level convergence anomalies over the tropical equatorial South America east of the Andes during drought years are consistent with low-level subsidence anomalies. This suggests anomalies in the upper and lower branches of the Hadley circulation over tropical South America east of the Andes, and of the Walker circulation over the equatorial Atlantic.

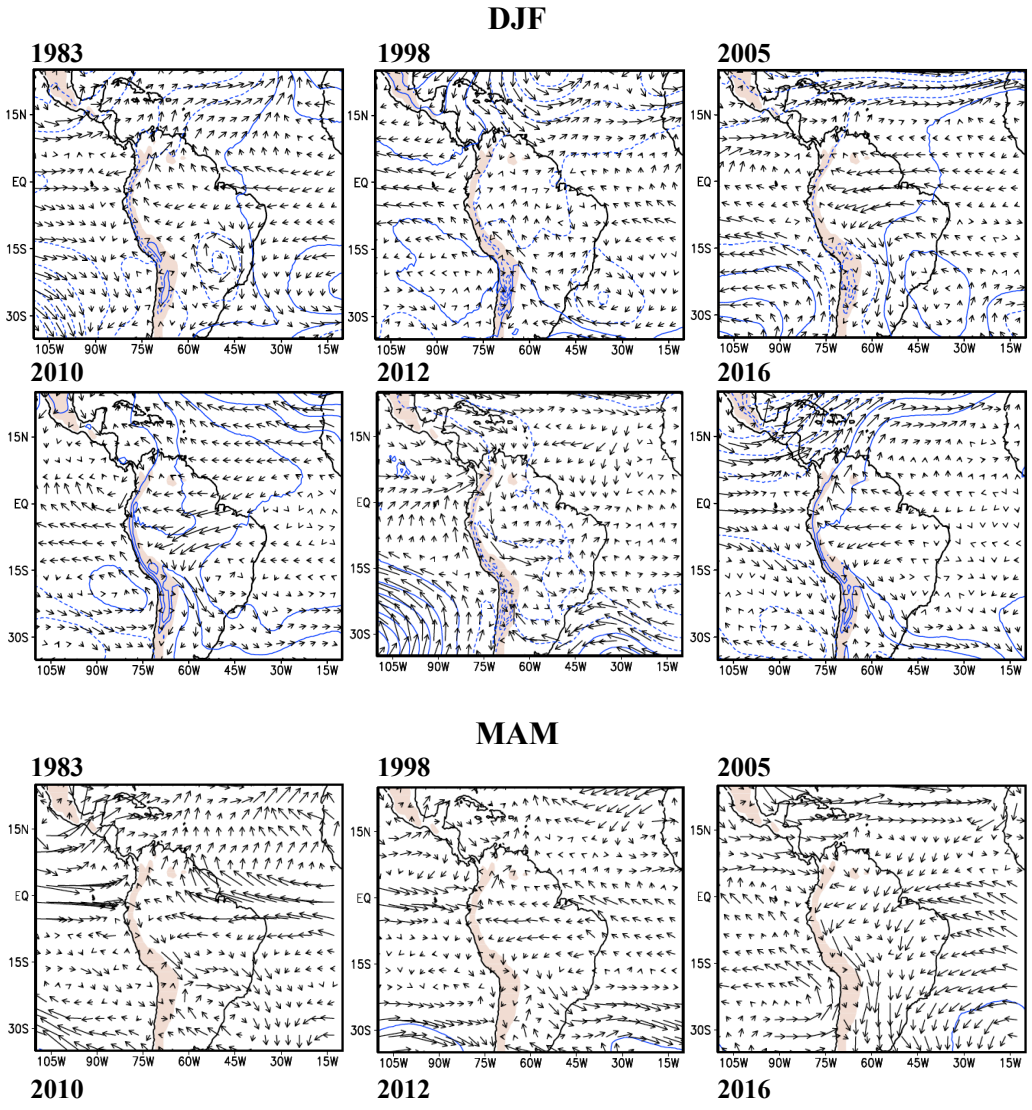

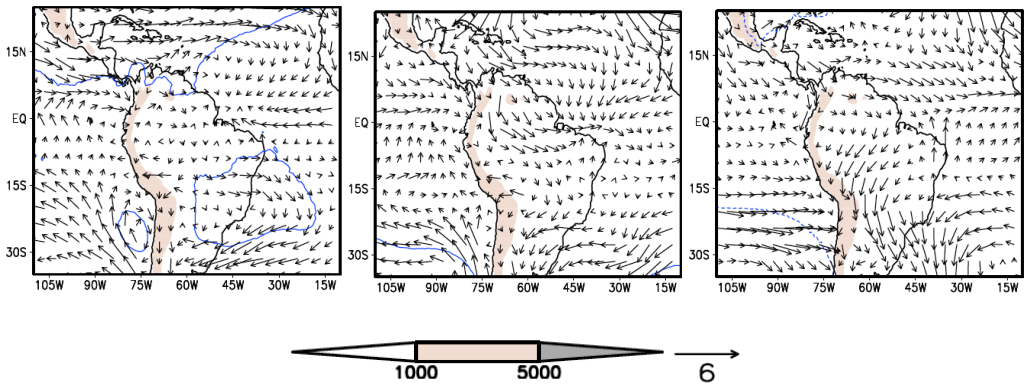

Figure x. Anomalies of wind (m/s) and geopotential height (m) anomalies at 850hPa for austral summer (DJF) and spring (MAM) during Amazonian droughts in 1983, 1998, 2005, 2010, 2012, and 2016. Solid (dot) blue lines represent anomalies of geopotential height in intervals of 50m (-50m). Brown shading represent topography of tropical Andes.

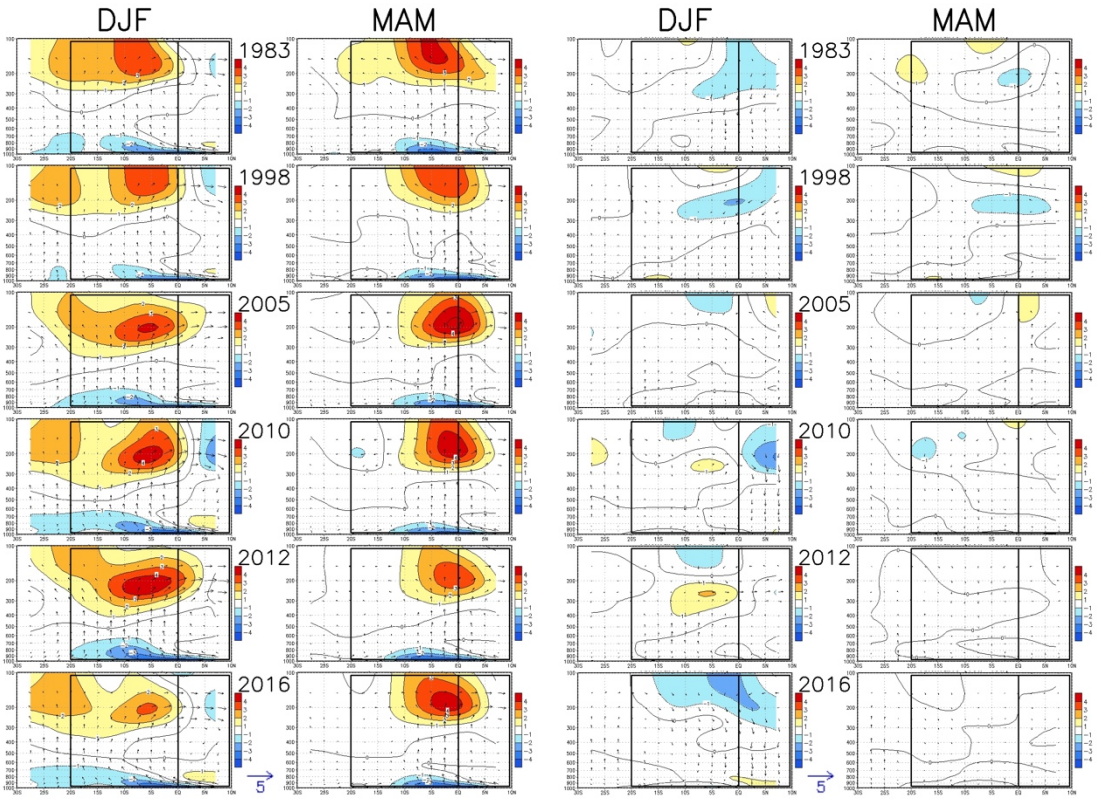

Figure x. Pressure-longitude section (10N-30S) of the mean (left) and anomalous (right) divergence (contour interval is 10^{-6} s^{-1}) and divergent circulation averaged between 65W-40W. The divergent circulation is represented by vectors of combined pressure vertical velocity and the divergent component of the zonal wind. Red shading and solid contours denote divergence (left) and anomalous divergence (right). Blue shading and dashed contours denote convergence (left) and anomalous convergence (right). Anomalies are departures from the 1981-2010 base period seasonal means. Black boxes delimitate southern Amazonia (including NEB) and northern Amazonia.

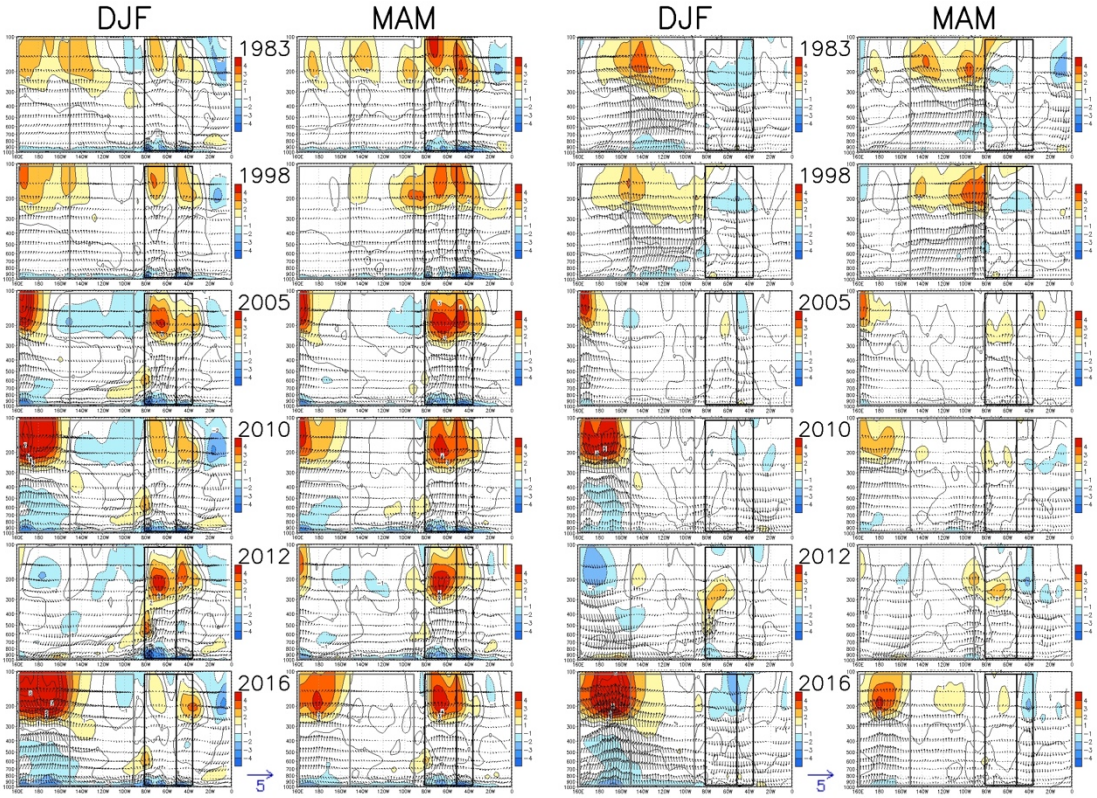

Figure 2x. Pressure-longitude section (0-160E) of the mean (left) and anomalous (right) divergence (contour interval is 10^{-6} s^{-1}) and divergent circulation averaged between 5N-5S. The divergent circulation is represented by vectors of combined pressure vertical velocity and the divergent component of the zonal wind. Red shading and solid contours denote divergence (left) and anomalous divergence (right). Blue shading and dashed contours denote convergence (left) and anomalous convergence (right). Anomalies are departures from the 1981-2010 base period seasonal means. Grey boxes delimitate EN4 and EN3 regions, and black boxes delimitate Amazonia and NEB regions.

DISCUSSION AND CONCLUSIONS

The impacts of droughts on Amazon and Northeast Brazil climate and ecosystems can be markedly different because of the nature and location of warming in the tropical Pacific and Atlantic oceans (e.g. if warming is detected in central or eastern Pacific), and in the location of the drought conditions across these regions.

Spatial patterns of drought over the Amazon region during the course of 1982-83, 1997-98 and 2015-16 were consistent with strong warming over the tropical Pacific during the austral summer DJF and to lesser extent during the next season MAM, but with different intensities and patterns between these three events. Warming during the DJF season in 1982-83 and 1997-98 was strong in both CP and EP regions, while during the MAM season the warming was more intense in the EP region. Although the recent 2015-2016 El Niño event was considered as strong as 1997-1998 in terms of SST anomalies, but it was characterized by strong warming in the CP region and warmest air temperatures over Amazonia were detected in 2016 (Marengo et al 2018).

Droughts conditions were also evidenced over the NEB region during the three EN events in 1982-83, 1997-98 and 2015-16, particularly during the wet season MAM. This region was also affected by drought in MAM 2005 and 2010, linked to anomalous warming over the TNA region. However, in these last two cases drought over NEB was focused over North NEB.

It is particularly remarkable the widespread drought over NEB in 2012 and prevailing wet conditions over Amazonia, when cold surface water were detected in EP and CP and almost near normal SST anomalies in TNA. Extreme rainfall in Amazonia created a compensatory subsidence pattern in Northeast Brazil that inhibited rainfall over that region in MAM (Marengo et al. 2013).

Therefore, the link between the spatial patterns of droughts and warm SST anomalies events could be explained because of the different contributions from CP, EP and TNA regions, characterized by different SST indices as shown in Figure 3. The highest EP anomalies were observed during 1982-83 and 1997-98, whereas the highest CP anomalies were observed in 2009-2010 and 2015-16. For the TNA region, there is an upward SST anomaly trend since the end of the 1990's and while TNA anomalies are not strong in 2012, the trends shown increase after that. TNA index was unusually high during 2010. In constrast to 2010, the 2015 drought emerged from a more complex combination of positive anomalies in the CP and TNA oceanic indices.

Impacts

The 2015-16 El Niño, which occurred under a global warming trend, imposed extreme warming and drought conditions over Amazonia (Jiménez-Muñoz et al., 2016), leading to a number of impacts. Fire incidence increased by 36% during the 2015-16 drought compared to the preceding 12 years, and this drought had the largest ever ratio of active fire counts to deforestation, with active fires occurring over an area of 799,293 km^2. Most strikingly, unlike the 2005 and 2010 droughts, active fire detections associated with the 2015 drought extended beyond the Arc of Deforestation in southern Amazonia (Aragao

et al 2018). As a consequence of increased fires in Amazonia, Gloor et al (2018) estimated that between July 2015 to June 2016 (compared with January 2011 to December 2011) there is a difference in the carbon releases by the fires of the order of 2.4 PgC. Furthermore, Mahli et al (2018) showed this event led to a record rate of rise of atmospheric CO_2 of 3.4 ppm in 2016, resulting in the mean global atmospheric CO_2 concentration staying above the symbolically significant value of 400 ppm for the entire year. One-quarter of this record rise was caused by the biosphere's response to the impacts of El Nino fires in 2015-16 (the rest was from direct anthropogenic emissions). The tropical biosphere was a key element in the reduction of the global land carbon sink observed during this EN event (Liu et al. 2017), with some studies suggesting a reduction on photosynthesis in late 2015 and an increase in respiration during early 2016 (Luo et al 2018). In particular, widespread reduction in sun-induced fluorescence over Amazon forests were observed during the 2015-16 El Niño, especially over the eastern part of the Amazon basin (Koren et al. 2018). These findings agree with the extreme drought observed over eastern/northeastern Amazonia during this period (Jimenez et al. 2018; Aragao et al 2018).

In Northeast Brazil, the El Nino in 2015-16 increased the effect of the drought that started in 2010. Because of losses in the agricultural, cattle ranching, water supply and local economies due to the drought, the federal government authorized the release of resources for the affected districts to mitigate these negative impacts (Marengo et al 2017). According to the Ministry of Integration (www.mi.gov.br), during 2012-2016, 33.4 million people were affected by the drought, with an estimated damage of R$ 104 billion (about US $ 30.0 billion).

ACKNOWLEDGEMENTS

This work was supported by the National Institute of Science and Technology for Climate Change Phase 2 under CNPq Grant 465501/2014-1, FAPESP Grant 2014/50848-9, the National Coordination for High Level Education and Training (CAPES) Grant 16/2014; …….

REFERENCES

Dee, D.P.; Uppala, S.M.; Simmons, A.J.; Berrisford, P.; Poli, P.; Kobayashi, S.; Andrae, U.; Balmaseda, M.A.; Balsamo, G.; Bauer, P.; et al. The ERA-Interim reanalysis: Configuration and performance of the data assimilation system. *Q. J. R. Meteorol. Soc.* **2011**, *137*, 553–597

Funk C, Peterson P, Landsfeld M, Pedreros D, Verdin J, Rowland J, Romero B, Husak G, Michaelsen J, and Verdin A. 2014. A quasi-global precipitation time series for drought monitoring. US Geological Survey Data Series 832. http://dx.doi.org/10.3133/ds832.

Nogueira SMC, Moreira MA, and Volpato MML. 2018. Evaluating precipitation estimates from Eta, TRMM and CHRIPS data in the South-Southeast region of Minas Gerais State-Brazil. Remote sensing, 10, 313. Doi:10.3390/rs10020313.

Paredes-Trejo FJ, Barbosa HA, Lakshmi Kumar TV. 2017. Validating CHIRPS-based satellite precipitation estimates in Northeast Brazil. Journal of Arid Environments, 139, 26-40. http://dx.doi.org/10.1016/j.jaridenv.2016.12.009.

Paredes-Trejo FP, Barbosa HA, and Spatafora LR. 2018. Assessment of SM2RAIN-derived and state-of-the-art satellite rainfall products over Northeastern Brazil. Remote Sensing, 10, 1093. Doi: 10.3390/rs10071093.

Sulca J, Takahashi K, Espinoza J-C, Vuille, M, and Lavado-Casimiro, W. 2017. Impacts of different ENSO flavors and tropical Pacific convection variability (ITCZ, SPCZ) on austral summer rainfall in South America, with a focus on Peru. International Journal of Climatology, 38(1), 420-435. https://doi.org/10.1002/joc.5185

Alvala RCS et al (2017) Drought Monitoring in the Brazilian Semiarid Region. An Acad Bras Ciencias. 89

Aragao LEOC (2018) 21st Century drought-related fires counteract the decline of Amazon deforestation carbon emissions, Nature Communications. 9:536 | DOI: 10.1038/s41467-017-02771-y | www.nature.com/naturecommunications.

Gloor E et al . (2018) Tropical land carbon cycle responses to 2015/16 El Nin˜o as recorded by atmospheric greenhouse gas and remote sensing data. Phil. Trans. R. Soc. B 373 : 20170302. http://dx.doi.org/10.1098/rstb.2017.0302

Jiménez-Muñoz JC, et al. (2016) Record-breaking warming and extreme drought in the Amazon rainforest during the course of El Niño 2015-2016. Sci. Rep. 6, 33130. (doi:10.1038/srep33130)

Jimenez-Muñoz, JC, et al. (2018) Spatio-temporal patterns of thermal anomalies and drought over tropical forests driven by recent extreme climatic anomalies. Phil. Trans. R. Soc. B. DOI:10.1098/rstb.2017-0300

Jimenez- Muñoz JC, , Takahashi K (2018) The role of ENSO flavours in recent droughts over Amazon forests, Poster presentation at the IV International Conference on El Nino Southern Oscillation: ENSO in a warmer Climate, 16-18 October 2018, Guayaquil. Ecuador.

Kalnay, E., M. Kanamitsu, R. Kistler, W. Collins, D. Deaven, L. Gandin, M. Iredell, S. Saha, G. White, J. Woollen, Y. Zhu, A. Leetmaa, B. Reynolds, M. Chelliah, W. Ebisuzaki, W. Higgins, J. Janowiak, K. C. Mo, C. Ropelewski, J. Wang, R. Jenne, and D. Joseph. The NCEP/NCAR 40-Year Reanalysis Project. Bulletin of the American Meteorological Society, March, 1996.

Koren G et al. (2018). Widespread reduction in sun-induced fluorescence from the Amazon during the 2015/2016 El Niño. Phil. Trans. R. Soc. B 373: 20170408.

Liu J, et al (2017). Contrasting carbon cycles responses of the tropical continents to the 2015-2016 El Niño. Science 358, eaam5690, doi:10.1126/science.aam5690.

Luo X, et al (2018). The impact of the 2015/2016 El Niño on global photosynthesis using satellite remote sensing. Phil. Trans. R. Soc. B 373, 20170409.

Malhi Y, et al (2018) New insights into the variability of the tropical land carbon cycle from the El Nino of 2015/2016. Phil. Trans. R. Soc. B 373 : 20170298.http://dx.doi.org/10.1098/rstb.2017.0298

Marengo, JA et al (2013). Two contrasting severe seasonal extremes in tropical South America in 2012: flood in Amazonia and drought in Northeast Brazil. J. Clim. 2, 9137–9154. doi: 10.1175/JCLI-D-12-00642.1

Marengo et al (2017) Climatic characteristics of the 2010-2016 drought in the semiarid Northeast Brazil region. An Acad Bras Cienc 89

Marengo JA et al (2018) Changes in Climate and Land Use Over the Amazon Region: Current and Future Variability and Trends. Front. Earth Sci. 6:228. Doi 10.3389/feart.2018.00228

Ropelewski C, Halpert M (1987) Global and regional scale precipitation patterns associated with the El Nino/Southern Oscillation, J. Climate, 115, 1606-1626.

Sulca J, et al. (2016) Impacts of different ENSO flavors and tropical Pacific convection variability (ITCZ, SPCZ) on austral summer rainfall in South America, with a focus on Peru. Int. J. Climatology 38(1), 420-435.

Takahashi K, et al. (2011) ENSO regimes: Reinterpreting the canonical and Modoki El Niño. Geophys. Res. Lett. 38, L10704.